

Improving the performance of light-emitting diodes via plasmonic-based strategies

EP

Cite as: J. Appl. Phys. **127**, 040901 (2020); doi: [10.1063/1.5129365](https://doi.org/10.1063/1.5129365)

Submitted: 27 September 2019 · Accepted: 9 January 2020 ·

Published Online: 27 January 2020



View Online



Export Citation



CrossMark

Xingce Fan,¹ Qi Hao,^{1,a)} Teng Qiu,¹ and Paul K. Chu^{2,3,4,a)}

AFFILIATIONS

¹School of Physics, Southeast University, Nanjing 211189, China²Department of Physics, City University of Hong Kong, Tat Chee Avenue, Kowloon, 999077 Hong Kong, China³Department of Materials Science and Engineering, City University of Hong Kong, Tat Chee Avenue, Kowloon, 999077 Hong Kong, China⁴Department of Biomedical Engineering, City University of Hong Kong, Tat Chee Avenue, Kowloon, 999077 Hong Kong, China^{a)}Authors to whom correspondence should be addressed: qihao@seu.edu.cn and paul.chu@cityu.edu.hk

ABSTRACT

Light-emitting diodes (LEDs), featuring long lifetime, small size, and low energy consumption, are increasingly popular for displays and general light sources. In the past decades, new light-emitting materials and novel device configurations are being continuously investigated to obtain highly efficient LEDs. Nevertheless, the unsatisfying external quantum efficiency severely limits their commercial implementation. Among all the approaches to boost the efficiency of LEDs, the incorporation of plasmonic structures exhibits great potential in increasing the spontaneous emission rates of emitters and improving the light extraction efficiency. In this Perspective, the methods to deal with challenges in quantum-well-based LEDs and organic LEDs by employing plasmonic materials are described, the mechanisms of plasmonic-based strategies to improve the light generation and extraction efficiency are discussed, and the plasmonic control over directional emission of phosphors is introduced as well. Moreover, important issues pertaining to the design, fabrication, and manipulation of plasmonic structures in LEDs to optimize the device performance, as well as the selection roles in finding appropriate plasmonic materials and structures for desired LED devices, are explained. This perspective lists the challenges and opportunities of plasmonic LEDs, with the aim of providing some insights into the future trends of plasmonic LEDs.

Published under license by AIP Publishing. <https://doi.org/10.1063/1.5129365>

I. INTRODUCTION

Light-emitting diodes (LEDs) are increasingly popular for displays and light sources because of the long lifetime, small size, and low energy consumption.^{1–3} Nowadays, most liquid-crystal-display televisions, computer monitors, and mobile phones are backlit with LEDs. In fact, they have essentially replaced traditional incandescent light bulbs commercially and are gaining ground on fluorescent tubes (bulbs) for general lighting applications as well. In the past few decades, low-dimensional quantum-well-based LEDs (QW-based LEDs) and organic LEDs (OLEDs) have been developed with extensive research activities on new light-emitting materials, novel device configurations, and extensions of the working wavelengths beyond the visible regime.

The external quantum efficiency (EQE) of an LED device is generally described by the production of internal quantum efficiency (IQE) and light extraction efficiency (LEE). IQE is strongly

influenced by nonradiative recombination processes, and is given by the ratio of radiative (k_{rad}) and nonradiative (k_{non}) recombination rates of the electron-hole pairs: $\text{IQE} = \frac{k_{rad}}{k_{rad} + k_{non}}$.⁴ Most LEDs suffer from the inherently low light-emitting efficiency due to low IQE, and several strategies have been proposed to improve the IQE values, such as growth of high-quality emissive crystals,⁵ management of singlet and triplet excitons of emitters,^{6,7} and incorporation of plasmonic structures.^{4,8,9} Among these methods, the introduction of plasmonic structures holds great promises in promoting IQE owing to its ability in manipulating spontaneous emission decay rates. Plasmonic structures provide strong charge density oscillations confined in the vicinity of plasmonic nanostructures.¹⁰ The collective oscillations, namely, localized surface plasmon resonance (LSPR) can be excited by an electrical field at the incident wavelength where resonance occurs, giving rise to intense confined electromagnetic fields.¹¹ When light-emitting materials are located

within the penetration depth of the localized surface plasmons (LSPs) fringing field, the emitted photons couple with the LSP modes instead of free space. The coupling leads to modified photon densities of states (DOSs) spurring spontaneous emission decay of emitters.^{4,12} As pointed out by Purcell, the effectiveness of modification on the spontaneous emission decay rate for a given wavelength depends on the photon DOS at that wavelength. The strongest enhancement occurs when the emission spectrum matches the LSPR energy, leading to a dramatically larger photon DOS. Consequently, the emitted photons can be recovered from the LSP modes and re-emitted into free space.¹³ The altered spontaneous emission decay rate of light-emitting materials results in reduced lifetime. The IQE* of LEDs with plasmonic structures can be revised as $\text{IQE}^* = \frac{\hat{k}_{\text{rad}} + C_{\text{ext}} k_{\text{lsp}}}{\hat{k}_{\text{rad}} + \hat{k}_{\text{non}} + k_{\text{lsp}}}$, where \hat{k}_{rad} and \hat{k}_{non} are the modified radiative and nonradiative decay rates, k_{lsp} is the LSPs' coupling rate, and C_{ext} is the probability of light extraction from the LSP modes decided by light scattering and electron vibration.⁴

Generally, the incorporation of plasmonic structures is extremely efficient in improving the IQE of emissive materials with low quantum efficiency, but it cannot help IQE exceed 100%. Hence, further optimization of LEDs is focused on the improvement of LEE. Due to the high total internal reflection in LEDs, a large portion of the generated light is confined in the device and finally dissipated. Only a small portion of light whose direction is within the escape cone can be extracted consequently.¹⁴ Nevertheless, when the plasmonic nanostructures are in resonance with the confined photons, efficient Mie scattering could change the propagation angles of photons thereby leading to higher probability of scattering photons out of the LEDs.¹⁵ On the other hand, metallic electrodes used to supply power in LEDs cover partial or even the entire LEDs surface. The surface plasmon polariton (SPP) modes form on the metallic electrodes and strongly confine the generated photons, resulting in strong energy dissipation. The confined modes that propagate along the metallic surface feature a relatively long lifetime. Appropriate design of plasmonic structures could help the photons be re-emitted into the free space, thereby improve the LEE.¹³

Construction of plasmonic structures on the phosphor layer to modify PL from the phosphor excited by the backlit LEDs is another approach to optimize LEDs performance, especially white LEDs.¹⁶ Generally, LSPRs supported by plasmonic structures present broadband optical responses and weak angular dependence and decay exponentially away from the plasmonic structures.¹⁷ But their optical response can be reinforced through coherent scattering when plasmonic materials are arranged in periodic arrays, leading to a collective plasmonic-photonic resonance termed as surface lattice resonance (SLR).^{18–22} The coupling of phosphors with SLR modes enables shaping of PL spectrum and angular emission enhancement of the phosphor layers, resulting in efficient luminescence in desired directions.^{23,24}

In this perspective, the challenges and opportunities of QW-based LEDs and OLEDs are presented, and the corresponding plasmonic-based strategies to improve the photon generation and extraction efficiency are discussed. The plasmonic control over directional emission of phosphors is also described. Important issues pertaining to design, fabrication, and manipulation of plasmonic structures in LEDs as well as the future trends of plasmonic LEDs are discussed.

II. PROMOTING LEDs EFFICIENCY BY PLASMONIC-BASED STRATEGIES

The characteristics of LSPR including resonance frequency and intensity of the LSPR absorption bands depend on the type of plasmonic materials, morphology, arrangement of nanostructures, and dielectric environment.²⁵ As shown in Fig. 1, noble metals such as Au and Ag are common plasmonic materials in the visible because of their large negative real part of permittivity and small imaginary part of permittivity at this range.¹⁰ The LSPR frequencies of Au can be tuned from the visible to the near-infrared (near-IR) regions, but extension of LSPR into the UV range is challenging owing to the dissipative channels induced by interband transitions at wavelengths shorter than 550 nm. Ag nanostructures support LSPR down to 360 nm, and it is generally employed as enhancement materials at near-UV region. Recently, Al with permittivity consisting of a large negative real and small positive imaginary component in the UV region has been suggested to be promising as a UV plasmonic material.^{26,27}

To address the problems in LED devices, tunable plasmonic materials with responsive spectra spanning a wide range from the UV to the near-IR are required to obtain effective LSP-exciton coupling and better LEE. Therefore, the plasmonic materials should be carefully chosen and appropriately designed to cater to the LED devices. In this section, the challenges and opportunities of plasmonic LEDs are discussed. Meanwhile, the plasmonic-based strategies for better LEDs performance are presented.

A. Plasmonic QW-based LEDs

1. Plasmonics in QW-based blue LEDs

In 2004, a pioneering work was reported by Okamoto *et al.* that Ag LSPs-enhanced blue InGaN/GaN QWs showed 14-fold enhancement in the photoluminescence (PL) peak and 6.8-fold improvement in the IQE.⁴ Other metals (Au and Al) have been incorporated into InGaN/GaN QWs, but IQE enhancement is not satisfactory because of the mismatch between the emission peaks and LSPR as shown in Figs. 2(a) and 2(b). Later on, they observed the effective coupling of LSPs and QWs by time-resolved PL.¹² They found that the decay profiles of Ag-coated InGaN/GaN QWs strongly depend on the wavelength and become faster at shorter

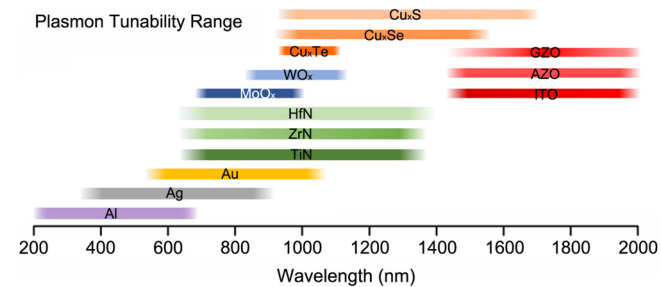


FIG. 1. Plasmon tunability range of metals, metal nitrides, metal oxides, metal chalcogenides, and doped conductive oxides.^{25–34}

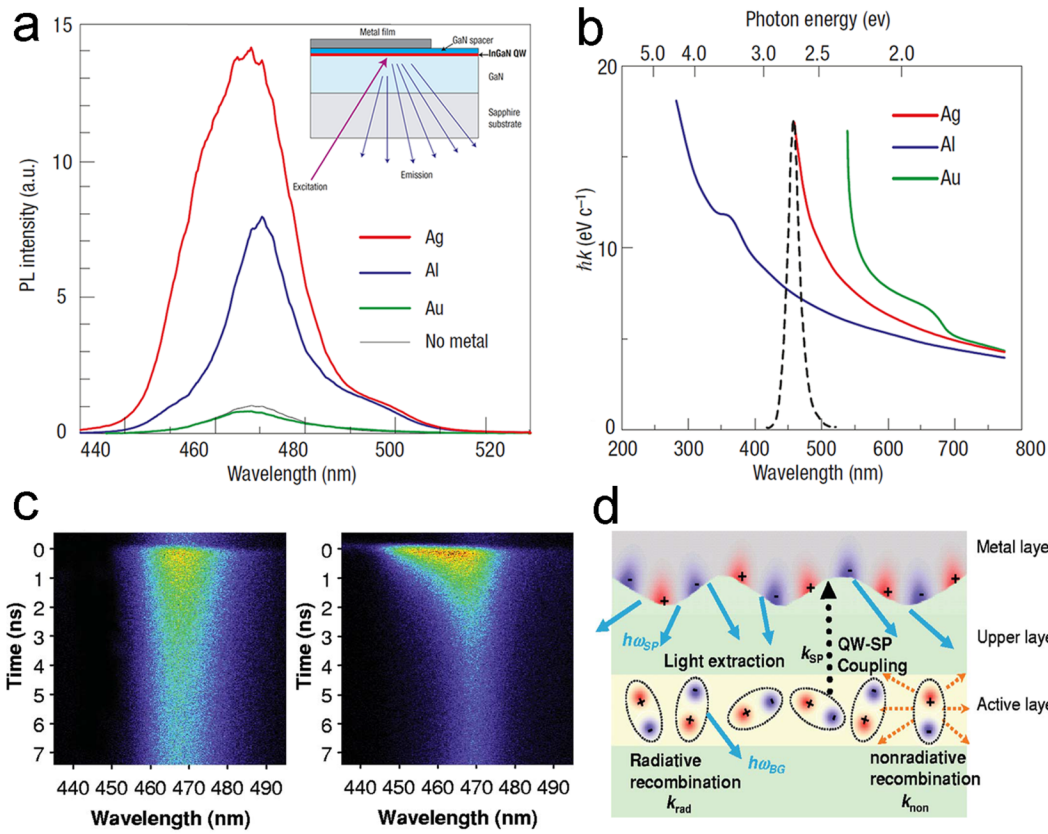


FIG. 2. (a) PL spectra of InGaN/GaN QWs coated with Ag, Al, and Au films. The inset of (a) shows the QW structure and excitation/emission configuration in the PL measurements. (b) Dispersion diagrams of the LSP modes on Ag/GaN, Al/GaN, and Au/GaN. The dashed line is the PL spectrum of InGaN/GaN. Reproduced with permission from K. Okamoto *et al.*, Nat. Mater. **3**, 601–605 (2004). Copyright Nature Publishing Group, 2004. (c) The temporal and spectroscopic profile of uncoated (left) and Ag-coated (right) InGaN/GaN QW probed by the Streak camera. (d) Schematic diagram of the electron–hole recombination and LSP-QW coupling mechanism. Reproduced with permission from K. Okamoto *et al.*, Appl. Phys. Lett. **87**, 071102 (2005). Copyright 2005 AIP Publishing LLC.

wavelength, whereas those of the uncoated sample show little spectral dependence, as shown in Fig. 2(c). A possible mechanism was proposed [Fig. 2(d)] that when the bandgap of InGaN layer is close to the electron vibration energy of LSPs, and when the emissive layer is within the penetration depth of LSPs fringing field, the emissive excitons in QWs transfer the energy to the LSPs, causing the faster decay of PL. Then, the LSPs lose momentum and couple to the radiated light, leading to enhanced PL. Moreover, the generated light is also scattered out of the LEDs by the coated Ag layer. Their results demonstrate the potential of plasmonic structures in addressing the existed problems in LEDs. It should be noted that the IQE enhancement of emitters by incorporating plasmonic structures is only effective for those with low IQE.

Currently, the EQE of commercial blue LEDs has exceeded 60%. The main challenge of high-performance blue LEDs is the EQE droop at high driving current and further reduction of its price. The significant EQE droop at high driving current was confirmed mainly due to the nonradiative Auger recombination and

the current overflow effect.^{35–37} In 2010, Lu *et al.*³⁸ demonstrated that effective coupling of LSPs with InGaN/GaN QWs could significantly reduce the droop phenomenon. The overlap of LSPs near field and QWs results in effective energy transfer from QWs to LSPs, generating an alternative emission channel even at high injection current density. The coupling leads to the significantly decreased density of carriers, thus suppressing the nonrecombination rates and EQE droop. Inserting a dielectric interlayer between the QWs and plasmonic structures could further strengthen the coupling between LSPs and QWs, resulting in a further reduction of EQE droop.³⁹ Although the high-performance blue LEDs have been achieved on sapphire or GaN substrate, further decrease in their price is held back by the unsatisfied IQE on much cheaper substrate, such as Si substrate.⁹ The low IQE is attributed to the presence of deep traps serving as nonradiative recombination channels. Further improvement of Si-based blue LEDs can be expected by the incorporation of plasmonic structures, where effective coupling of LSPs with QWs opens an alternative radiative recombination route to improve the IQE of Si-based LEDs.

2. Plasmonics in QW-based green LEDs

In the past decades, the QW-based blue and red LEDs have been well developed for commercial usage. However, green LEDs are seriously limited by the fundamental difficulty associated with the growth of InGaN/GaN QWs with high In composition.⁴⁰ The increase in In composition may cause chemical inhomogeneity of the InGaN well layers due to the poor miscibility between InN and GaN and the misfit strain-induced defects due to the large lattice mismatch between InGaN wells and GaN barriers. When the size of In phase segregation is above the critical value, large amounts of structural defects within the InGaN well layers seriously reduce the intensity of main peak and act as nonradiative recombination sites, causing the decrease of IQE.⁴¹ Another important issue concerning the IQE decrease of In-rich InGaN/GaN is the built-in piezoelectric polarization caused by strain in QWs, where the quantum-confined Stark effect (QCSE) reduces the wavefunction overlap between electrons and holes, leading to a strong decrease of radiative recombination rates and a redshift of emission wavelength.⁴²

When carriers are supplied to QWs with a built-in piezoelectric field, the carrier screening effect could reduce the QCSE leading to the blueshifted spectrum and increased radiation efficiency. In 2007, Chen *et al.*⁴² demonstrated that the QCSE

screening effect at a high carrier injection condition not only contributes to the emission enhancement, but also increases the LSP-QW coupling. Later on, Cho *et al.*⁴³ reported the reduction of QCSE by the Au LSP-coupling effect in the InGaN-based green LED [shown in Figs. 3(a) and 3(b)]. They analyzed the contribution of LSP-coupling to the QCSE in LEDs by excitation power-dependent PL and current-dependent electroluminescence (EL) measurements. As shown in Figs. 3(c) and 3(d), the blueshifts of PL and EL of the green LED with Au nanoparticles (NPs) are much smaller than those of the conventional green LED without Au NPs due to the compensation of the built-in piezoelectric field with the LSP-enhanced local fields of Au NPs. These results indicate that the incorporation of plasmonic structures in In-rich InGaN/GaN QWs could significantly enhance the output power of green LEDs and compensate the influence brought by the QCSE simultaneously. The so-called “green-gap” in EQE of QW-based LEDs may be bridged by the plasmonic effect.

3. Plasmonics in QW-based UV LEDs

UV LEDs have potential applications in air and water purification, medical phototherapy, and pumping source of white LEDs. The device performance of UV LEDs strongly depends on their

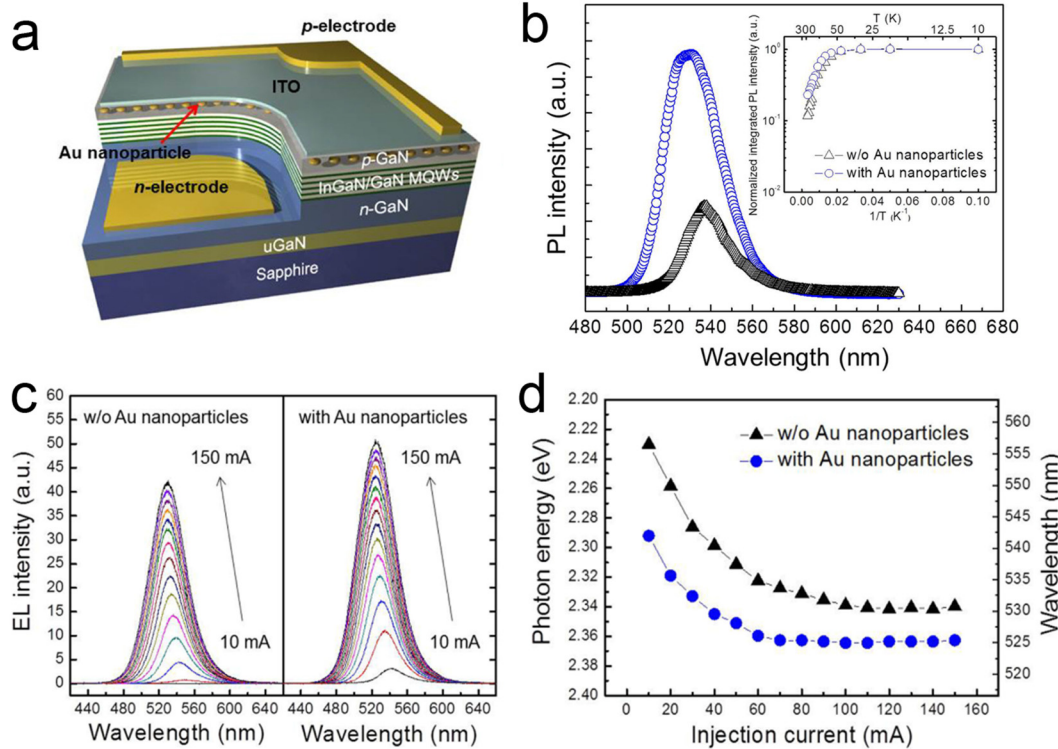


FIG. 3. (a) Schematic diagram of the structure of plasmonic green LEDs with Au NPs embedded in the p-GaN layer. (b) PL spectra of InGaN/GaN QWs with and without Au NPs. The inset shows the temperature-dependent integrated PL intensity of the QWs with and without Au NPs. (c) EL spectra of plasmonic green LEDs with and without Au NPs measured with increasing injection current at room-temperature. (d) EL emission wavelength of plasmonic green LEDs with and without Au NPs as a function of injection current. Reproduced with permission from C. Y. Cho *et al.*, Opt. Express **24**, 7488–7494 (2016). Copyright 2016 Optical Society of America.

emission wavelength. Since the InGaN-based near-UV emitters (400–365 nm) utilize fundamentally the same materials and device technologies as blue LEDs, they have profited from many years of large-scale industrial development. Therefore, the near-UV LEDs exhibit performance levels close to those of blue LEDs with EQE ranging from 46% to 76%.⁴⁴ However, there is a big drop in EQE of UV LEDs with emission wavelength shorter than 365 nm owing to the transition from InGaN- to AlGaN-based LED technologies. AlGaN, alloyed by GaN and AlN, is one of the most popular group-III nitrides used for fabricating UV LEDs due to its superior properties, such as direct bandgap, high emissive efficiency of short wavelength light covering almost entire UV region (210–400 nm), high electron mobilities, and high thermal conductivities.⁴⁵ So far, the practical applications of AlGaN-based LEDs have been hampered by its low EQE that is typically below 6%. One major reason for the low efficiency of AlGaN-based LEDs is the high density of nonradiative defects produced during material fabrication.

It has been reported that LSPs-coupling with InGaN-based QW-based LEDs leads to enhanced PL and EL intensity by improving the IQE.⁴⁸ To accomplish better LSPs-exciton coupling at the UV region, plasmonic materials presenting LSPR in the UV region

are needed. Ag is still a reasonably good plasmonic material at near-UV range, but it can only support LSPR down to ~360 nm. Recently, Al is regarded as the best candidate of UV plasmonic materials, which brings abundant opportunities for UV LEDs.^{26,27} In 2013, Cho *et al.*⁴⁶ demonstrated the improved optical output power of LSPs-enhanced AlGaN-based UV LEDs grown on the Si (111) substrate using an Al enhancement layer. The Al layer was selectively deposited close to the multiple QWs such that the induced near fields around the Al layer could strongly interact with the QWs. As shown in Figs. 4(a) and 4(b), the LSPs-enhanced UV LEDs with an Al layer showed 45% higher light output than a conventional UV LEDs without an Al layer at 700 mA; a peak pulsed power of 1.2 mW was achieved at a UV emission of 346 nm. The large enhancement of optical output power is attributed to improvement of IQE in multiple QWs resulting from the increased spontaneous emission rates by the LSPs-QWs coupling. Later on, He *et al.*⁴⁷ reported 2.6-fold enhancement in deep-UV emission of 292 nm from AlGaN multiple QWs by introducing Al NPs into the device [Fig. 4(c)]. Compared to the bare QWs, 2.3-fold enhancement in the IQE (from 16% to 37%) and 13% enhancement in LEE have been observed from multiple QWs decorated with Al NPs due

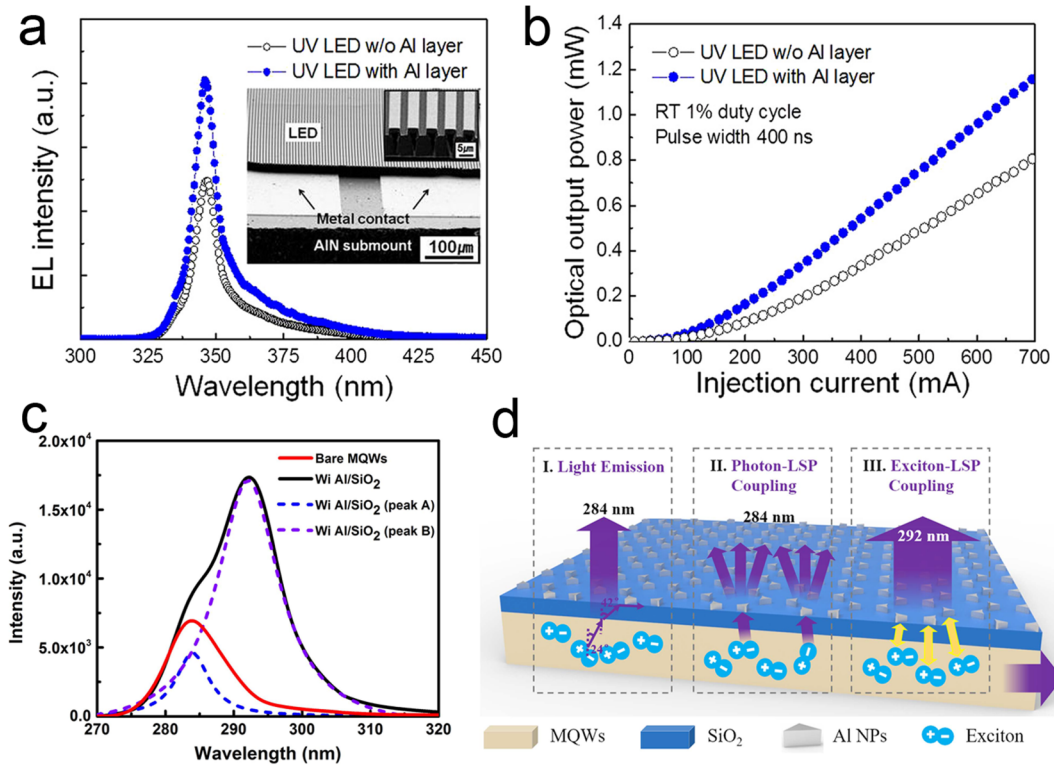


FIG. 4. (a) Room temperature EL spectra of UV LEDs with and without Al layer. The inset shows inclined plan-view SEM images of plasmonic UV LEDs. (b) The optical output power of UV LEDs with and without Al layer as a function of injection current. Reproduced with permission from C. Y. Cho *et al.*, Appl. Phys. Lett. **102**, 211110 (2013). Copyright 2013 AIP Publishing LLC. (c) PL spectra of AlGaN QWs with and without the Al/SiO₂ composite structure (solid lines) at room temperature, and the multimodal Lorentz fitting of the AlGaN QWs with Al/SiO₂ composite structure (dashed lines). (d) Schematic diagram of light emission in AlGaN QWs with Al/SiO₂ composite structure. Reproduced with permission of J. He *et al.*, Nanotechnology **29**, 195203 (2018). Copyright 2018 IOP Publishing.

to the improved IQE as well as effective Mie scattering of Al NPs [Fig. 4(d)]. The examples underline that the incorporation of appropriate Al plasmonic structures into deep-UV LEDs is significantly efficient to optimize the device performance by generating effective LSPs-exciton coupling and increasing LEE. To push the EQE of AlGaN-based deep-UV LEDs reaching the level of commercial use, enormous endeavor should be paid to improve the performance. We believe that the incorporation of Al plasmonic structures could contribute as an alternative route for a better performance of deep-UV LEDs.

B. Plasmonic OLEDs

OLEDs have received great attention as potential next-generation displays due to their low power consumption, excellent color gamut, fast response time, and especially their flexibility.^{49,50} Currently, most emitters of OLEDs are inefficient in light-emitting properties. It is the same with QW-based LEDs that the IQE of OLEDs can be enhanced by the plasmonic effect. Suitable plasmonic materials and structures always need to be well designed for

maximizing the OLEDs efficiency. As shown in Fig. 5(a), Xiao *et al.*⁵¹ dispersed the Au NPs into the hole transport layer with the proper ratio. The LSPR band of the Au NPs overlaps the emission of green emitters [Figs. 5(b) and 5(c)], and an increase of 25% in the EL intensity is observed from the OLEDs with Au NPs, whereas the spectral and electrical properties maintain the same as those of the reference device. In another study, the synergistic effects of different plasmonic NPs are confirmed and exploited to boost the IQE and LEE simultaneously.⁵² As shown in Fig. 5(d), the OLEDs are doped with either Au or Ag or both Au and Ag NPs, and EL measurements show that the codoped OLEDs exhibit the largest EL enhancement. Both the Au and Ag NPs contribute to the enhancement of IQE, whereas the improved LEE is mainly caused by scattering of Ag NPs. Since the higher Mie scattering efficiency leads to the propagation angle change of the confined light [Fig. 5(e)], thus leading to a higher probability of scattering light out of the device.

In the past decade, great endeavors have been paid to develop emitters with high quantum yields. Especially, perovskite quantum dots (QDs) APbX_3 [$\text{A} = \text{CH}_3\text{NH}_3^+$ (MA) and Cs; X = I, Br, Cl] as a

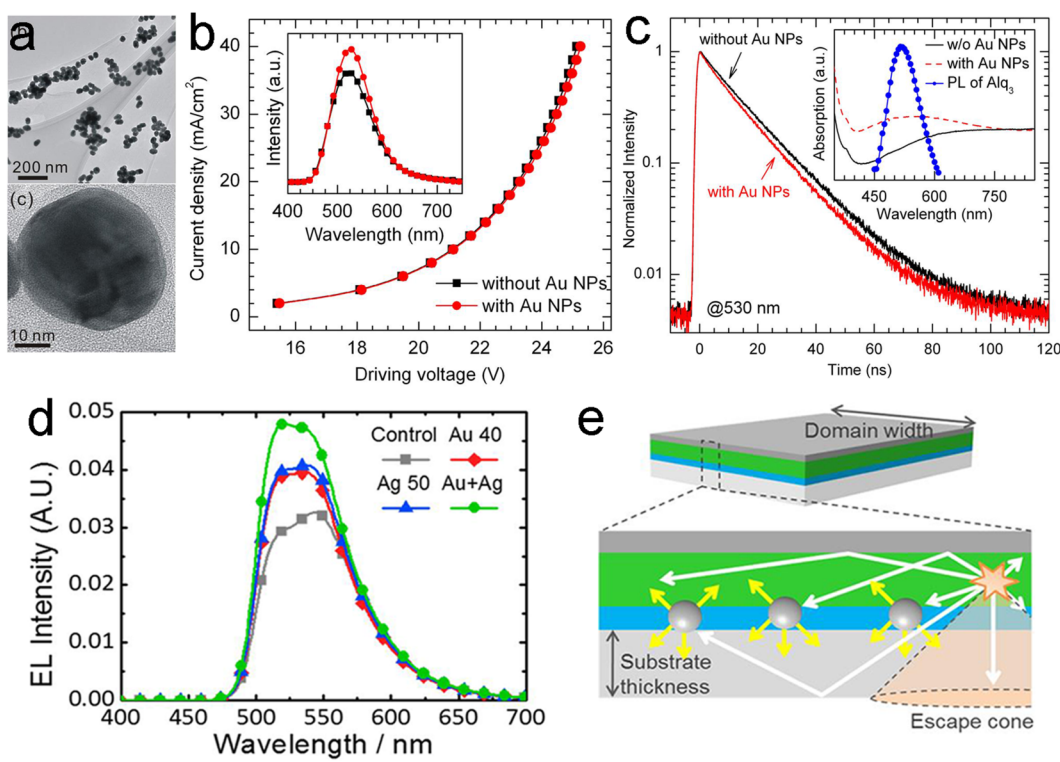


FIG. 5. (a) TEM and HR-TEM images of the chemically synthesized Au NPs. (b) Current density-voltage characteristics of the OLEDs with and without Au incorporation. The inset shows the EL spectra at a current density of 40 mA cm^{-2} . (c) Time-resolved PL spectra acquired at a wavelength of 530 nm using a 370 nm laser source. The inset shows the absorption spectra of the carrier injection layer with and without Au NPs on the ITO-glass substrate together with the PL spectrum of the emissive layer. Adapted with permission from Y. Xiao *et al.*, Appl. Phys. Lett. **100**, 013308 (2012). Copyright 2012 AIP Publishing LCC. (d) EL spectra of the OLEDs (as-prepared, doped with either Au or Ag, and both Au and Ag NPs) at a constant current density of 5 mA cm^{-2} . (e) The schematic diagram of the metal-NPs-doped OLEDs with enhanced LEE by scattering light out of the device. Adapted with permission from C. Cho *et al.*, ACS Appl. Mater. Interfaces **8**, 27911–27919 (2016). Copyright 2016 American Chemical Society.

new class of optoelectronic semiconductors have been used in LEDs because of the long free-carrier diffusion length, high carrier mobility, tunable bandgap, high PL quantum yield, as well as solution processability.^{53–55} Nevertheless, their unstable properties in the air need to be addressed prior to commercialization. Although the perovskite QDs are of high quantum yields, it still leaves space for the improvement of IQE by the plasmonic effect.^{56–59} The first report demonstrating the improved performance of perovskite QD-based LEDs by the plasmonic effect was by Zhang *et al.* who synthesized Ag nanorods exhibiting LSPR in the visible range.⁵⁸ To maximize the enhancement ratio, Ag nanorods with an LSPR peak of 525 nm were uniformly dispersed into the hole transport layer of the LEDs to match the green emission peak of CsPbBr₃ QDs (527 nm). The results show that EL was enhanced by a factor of 42% from the device composed of Ag nanorods as a result of efficient LSP-exciton coupling between the CsPbBr₃ QDs and Ag nanorods.

Although almost 100% IQE of OLEDs has been achieved, the EQE is still limited due to poor light extraction. In OLEDs, the metallic electrodes are needed to cover the entire surface to inject sufficient carriers. In this case, the SPP modes excited on metallic electrodes and the accompanied waveguide modes generally confine a large portion of generated photons, resulting in strong energy dissipation.¹⁴ The confined photons have a relatively long lifetime and can be re-emitted into free space by designing appropriate structures. Owing to the nonradiative properties of SPPs, it is difficult to extract light from flat metal-dielectric interfaces. Introduction of plasmonic structures with LSPR properties leads to efficient light out-coupling and can be implemented to extract light from either the cathode or anode side for top-emitting and bottom-emitting LEDs, respectively. Top-emitting LEDs are particularly suitable for displays because the driving circuits of the pixel/matrix can be integrated into the substrate without reducing the window size or throughput.¹³ The generated light can be extracted from the opaque metallic cathode by the cross-coupling effect.⁶⁰ As shown in Fig. 6, the initially excited LSP modes at the dielectric-metal interface (interior) can be cross-coupled with the LSP modes at the opposite metal-dielectric interface (exterior) and so photons can be re-emitted into free space by the exterior LSP modes. In bottom-emitting LEDs especially OLEDs, introducing micro-/nanopatterns with random or periodic morphologies to the metallic electrode-organic interfaces has been demonstrated to recover the photons from the trapped SPP modes.^{61–69} The photons trapped in the waveguide modes can also be recovered simultaneously when the Bragg-scattering condition is satisfied on the periodic cathode (Fig. 7).⁶⁴

C. Plasmonic control over the directional emission of phosphors

Currently, the leading commercial methodology for white lighting generation is still based on the blue LEDs-excited PL of yttrium aluminum garnet doped with Ce³⁺ (YAG:Ce) phosphor. The rare-earth-ions-based phosphors typically have low absorption coefficients in the blue region, resulting in that the thickness of phosphors is of several tens of micrometers. The randomly scattered light in the phosphor layer typically presents the Lambertian

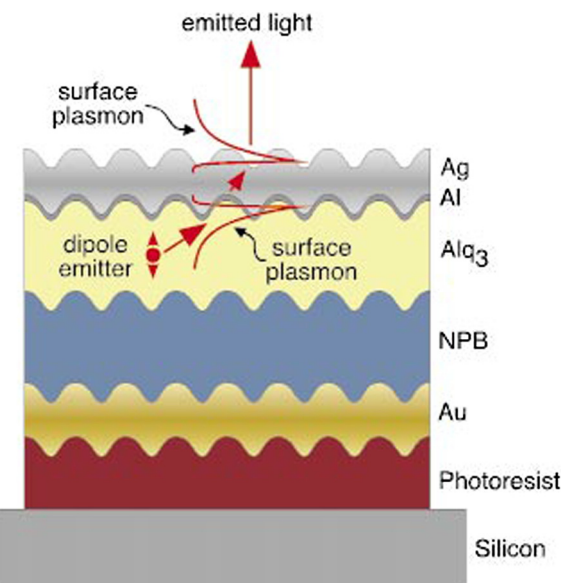


FIG. 6. Schematic diagram of light extraction from the top-emission OLEDs by the cross-coupling effect. Reproduced with permission from D. K. Gifford *et al.*, Appl. Phys. Lett. **81**, 4315–4317 (2002). Copyright 2002 American Institute of Physics.

emission profile.^{70,71} In this case, nearly half of the extracted light from the phosphor layer is backscattered and external secondary optical elements are needed for the maximum light output, leading to light loss. In other applications such as automotive lighting and light guide in screens, the highly directional lighting sources are typically required.¹⁶ Hence, directional control over the emission of the phosphor layer is fascinating for promoting light output efficiency and catering to the demands of practical applications.

As discussed in the Introduction, when plasmonic NPs are arranged in periodic arrays, such coherent scatterings lead to the SLR. It is quite different from the LSPR that the in-plane scattering by the plasmonic NPs and phase accumulation of these scattered fields govern the optical response of SLR, presenting sharp resonance peaks and extremely low radiation loss.²⁰ Moreover, the field enhancement of this resonance extends over a much larger distance in the space between the nanoantennae [as shown in Figs. 8(a) and 8(b)], leading to its ability to enhance dye emission from much larger volumes compared with the case of LSPR.^{17,18} SLR can couple very efficiently to radiation because of their hybrid plasmonic-photonic characters. In 2013, Lozano *et al.*¹⁷ designed a periodic Al nanoantennae array that supports SLR modes. After the integration of dye molecules onto the Al nanoantennae array, a 70-fold directional enhancement for p-polarized emission and 60-fold enhancement for unpolarized emission of dye molecules are demonstrated [Fig. 8(c)]. The resonant excitation of the emitters was confirmed to contribute to the overall angle-dependent enhancement. Moreover, the SLR supported by plasmonic structures enables the shaping of PL spectrum and

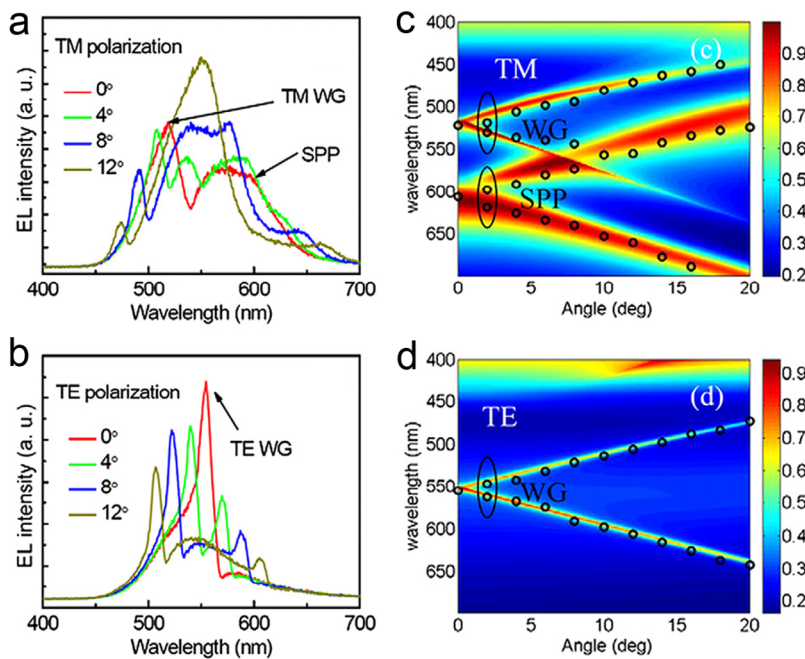
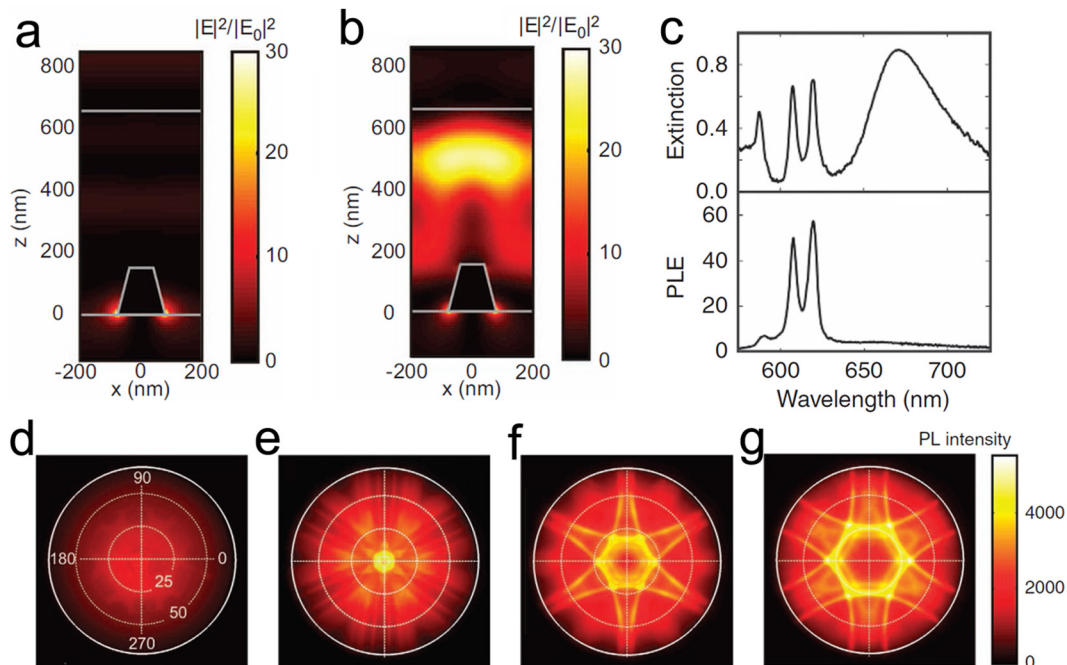


FIG. 7. Measured EL spectra with (a) TM and (b) TE polarization at different observation angles from the corrugated OLEDs with 350-nm grating. The wavelength vs incident angle for the calculated dispersion relation of the corrugated OLEDs for (c) TM and (d) TE polarization. The measured dispersion relation extracted from the EL spectra (marked as circles) is also shown in (c) and (d). Reproduced with permission from Y. Bai *et al.*, *Org. Electron.* **12**, 1927–1935 (2011). Copyright 2011 Elsevier B.V.



angular pattern of the emission from the emitters. In this case, the enhancement of spatial coherence of emission leads to that most light is beamed into a very narrow angular range in a defined direction, resulting in the angle-dependent enhancement. Afterward, they combined these structures with high-power standard blue LED sources, showing that the plasmonic structure acts as an integrated optical component to shape the emission pattern of the phosphor layer. Later on, they demonstrated an enhanced and tailor-made directional emission of light-emitting devices using nanoimprinted hexagonal arrays of Al NPs.²³ The separation of the Al NPs in the array yields an accurate angular distribution of the emission as shown in Figs. 8(d)–8(g). Such a novel design of plasmonic arrays allows control over light emission without requiring external secondary optical components. However, the directional control over the emission by plasmonic structures is generally accompanied by the altering of intensity and shape of the phosphor PL spectrum. For production of directional white lighting source, the plasmonic structures as well as the phosphor layers need to be carefully designed.

III. NANOFABRICATION OF PLASMONIC NANOSTRUCTURES

As reported by Okamoto *et al.* in 2004, the incorporation of a silver layer increases the spontaneous recombination rates of emitters resulting in large IQE enhancement.⁴ However, the structure may be impractical for real devices because the thin GaN spacer leads to ineffective carrier injection and inferior ohmic contact. The Ag layer on the p-GaN layer decreases the LEE of device on account of SPPs loss in the flat Ag layer, and moreover, the light generated from the LEDs is blocked by the opaque Ag layer. To address these problems, plasmonic nanostructures with tunable LSPR responses are adopted and different nanofabrication methods have been proposed. In this section, the nanofabrication methods of plasmonic nanostructures on LEDs are classified into two categories, NPs and nanoarrays.

Solution-based chemical synthesis and solid state dewetting (SSD) are efficient in the fabrication of plasmonic NPs. While plasmonic nanoarrays are often fabricated in combination with vacuum deposition with lithography or template-assisted assembly, such as electron beam lithography (EBL), interference lithography, imprint lithography, nanosphere lithography, and hard-template-assisted lithography. Because of different materials and configurations of LED devices, a suitable incorporation method of the plasmonic structure should be selected to cater to a better device performance.

In this section, we not only focus on the topic of several practicable nanofabrication methods to incorporate plasmonic nanostructures into LED devices, but also discuss their compatibility in different types of LEDs. These nanofabrication methods offer good solutions to energy match between LSPs and hot excitons by tuning the LSPR properties of the plasmonic structures. The high-performance LEDs also benefit from advanced nanotechnologies owing to the improved LEE. Moreover, the precise construction of periodic plasmonic nanoarrays supported SLR is also discussed for acquiring directional emission enhancement from the phosphor layer.

A. Chemical synthesis

The plasmonic NPs with well-defined shapes, such as spheres, spheroids, cubes, plates, and rods, are generally prepared by chemical synthesis approach.⁷² The position and intensity of the LSPR bands can be tuned by altering the size, shape, or dielectric environment. The flexible tuning of LSPR frequency enables the precise energy matching with the hot excitons of emissive materials and sometimes generates an efficient light scattering to boost LEE.^{73,74}

Spin-coating, drop-casting, or spray process are usually adopted to disperse plasmonic NPs on functional layers of QW-based LEDs;⁷⁵ however, the aggregation of plasmonic NPs needs to be addressed so as to avoid unsatisfied enhancement of device performance. The chemically synthesized plasmonic NPs could greatly benefit the OLEDs owing to the facile incorporation method of mixing them up into the functional layers, e.g., carriers injection layers. The effective LSP-exciton coupling alters the spontaneous decay rates of emitters and sometimes leads to a better LEE by Mie scattering of plasmonic NPs.⁷⁶

B. Solid state dewetting

In QW-based LEDs, the light-emitting structures are typically fabricated by molecular beam epitaxy, chemical vapor deposition, or other methods requiring a thermal treatment to reduce defects, and therefore, it is convenient to combine vacuum deposition with postannealing to fabricate plasmonic NPs for QW-based LEDs. This process is always termed as solid state dewetting (SSD) in which particles are formed when the solid matters are heated to a sufficiently high temperature but below the melting point.^{77–80}

Kwon *et al.*⁸ inserted a layer of Ag NPs between the InGaN/GaN QWs and n-GaN layer by vacuum deposition and postannealing (as shown in Fig. 9). The optical output power of the LEDs with Ag NPs is 32.2% higher than that of LEDs without Ag NPs for an input current of 100 mA. Besides, large Ag NPs have also been embedded in the ITO transparent anode by thermal treatment of small spin-coated Ag NPs.⁸¹ Although the ITO layer with Ag NPs is 150 nm above the InGaN/GaN multiple QWs, the output power is 1.8 times that of conventional LEDs at 350 mA. The enhanced device performance is ascribed to strong light scattering of the plasmonic Ag NPs embedded in the ITO anode.

Although the SSD process is facile to incorporate plasmonic NPs into the LEDs device, the precise control of the LSPR of plasmonic structures on LEDs is challenging. Because the SSD process is highly sensitive to the surface morphology of underlying substrates, the SSD process always produces randomly dispersed plasmonic NPs on the unpatterned surface.⁷⁹ Figure 9(b) depicts the dewetted Ag NPs arrays on the patterned Si substrate with highly ordered surface morphology.⁸² Therefore, SSD on the well-patterned surface, such as patterned ITO anode, would be one of the good solutions to precisely manipulate LSPR of plasmonic NPs in LEDs.

C. Electron beam lithography

Electron beam lithography (EBL) is efficient in controlling the particle size, shape, and interparticle distance accurately. The spatial resolution of plasmonic nanoarrays patterned by EBL

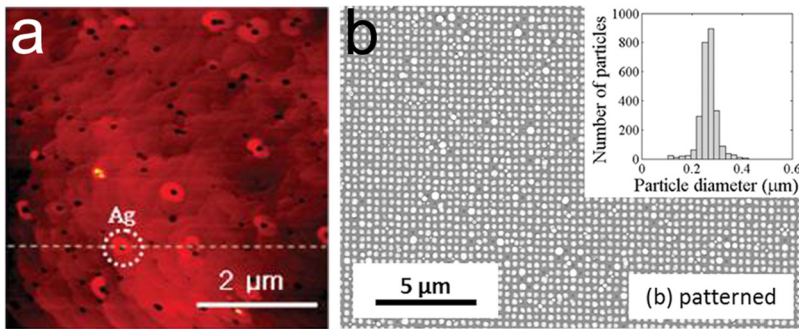


FIG. 9. (a) AFM image of Ag NPs deposited on the n-GaN layer after thermal annealing. Reproduced with permission from M. K. Kwon *et al.*, *Adv. Mater.* **20**, 1253–1257 (2008). Copyright 2008 WILEY-VCH Verlag GmbH & Co. KGaA, Weinheim. (b) A SEM image of a 26 nm thick Ag layer deposited on a patterned substrate after annealing. Reproduced with permission from A. Le Bris *et al.*, *Appl. Phys. Lett.* **105**, 203102 (2014). Copyright 2014 AIP Publishing LLC.

reaches the sub-10 nm level, thus enabling the precise control of the LSPR frequencies. Typically, the EBL process involves spin-coating of electron-sensitive photoresist, electron beam patterning, photoresist development, materials deposition, and removal of residual photoresist. As shown in Fig. 10, Lu *et al.*⁸³ used the EBL to pattern Ag nanoarrays on the p-GaN cladding layers of InGaN/GaN multiple QWs to overcome the limitations of the exponentially decaying LSPR field of Ag nanostructures without sacrificing the thickness of the p-GaN layer. A 2.8-fold enhancement in the PL intensity and improved LEE have been achieved simultaneously.

Moreover, EBL allows high resolution construction of plasmonic nanoarrays on the phosphor layer of some LEDs with well-defined shape, size, and arrangement of NPs, enabling the

precise tuning over SLR properties of plasmonic nanoarrays to generate desired angular enhancement of emission from phosphors. Although EBL provides a powerful tool to manipulate plasmonic structures in LEDs device, the large-scale fabrication may be hampered by its low throughput and high cost. There are alternative methods for high-resolution nanoarrays patterning on LEDs device, such as interference lithography, imprint lithography, and template-assisted assembly. These methods could produce plasmonic nanoarrays with adequate spatial accuracy at a much lower cost and a high-throughput, boding well for commercialization.

D. Interference lithography and imprint lithography

In OLEDs system, the metallic electrode can be patterned with appropriate structures to diminish the energy dissipation caused by plasmonic and waveguide modes. Generally, the micro-/nanopatterns on the metal cathode are replicated from the patterned anode or organic functional layers. Interference lithography and imprint lithography techniques are commonly used to construct the periodic patterns.

Interference lithography begins with exposing the spin-coated photoresist on the anode (substrate), and after development, reactive ion etching is conducted to create patterns on the anode. After the removal of residual photoresist, the organic functional layers and metal cathode are then constructed layer-by-layer. Alternatively, Jin *et al.*⁶⁶ directly created the patterned photoresist on the anode without reactive ion etching [Figs. 11(a)–11(c)] to simplify the fabrication process. Since most polymers are sensitive to UV laser ablation due to the low UV power threshold, the corrugated morphology can be directly recorded on the organic functional layers of OLEDs by laser ablation. Bai *et al.*⁶⁴ demonstrated one-step laser ablation of the hole transport layer of OLEDs and the corrugated morphology was duplicated on the metallic cathode. Better EL efficiency was observed from the corrugated OLEDs because of out-coupling of the confined SPPs and waveguide modes simultaneously.

Another approach to create a corrugated morphology on the cathode is imprint lithography. High-spatial-resolution patterning of organic functional layers can be performed by thermal, vacuum, and UV imprinting. Liu *et al.*⁶⁹ designed a nanostructured electrode in the OLEDs by vacuum imprint lithography as shown in Figs. 11(a), 11(b), and 11(d)–11(g). The gratinglike patterns on the

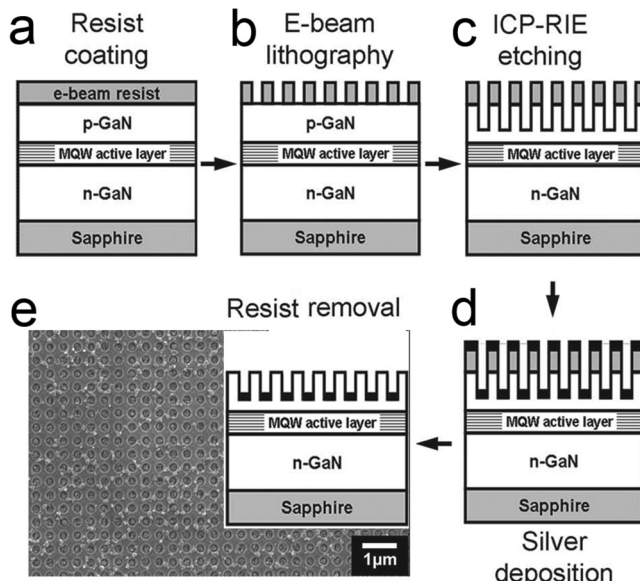


FIG. 10. (a)–(e) Schematic illustrations of using EBL to pattern Ag nanoarrays on the InGaN/GaN multiple QWs. Reproduced with permission from C. H. Lu *et al.*, *Adv. Funct. Mater.* **21**, 4719–4723 (2011). Copyright 2011 WILEY-VCH Verlag GmbH & Co. KGaA, Weinheim.

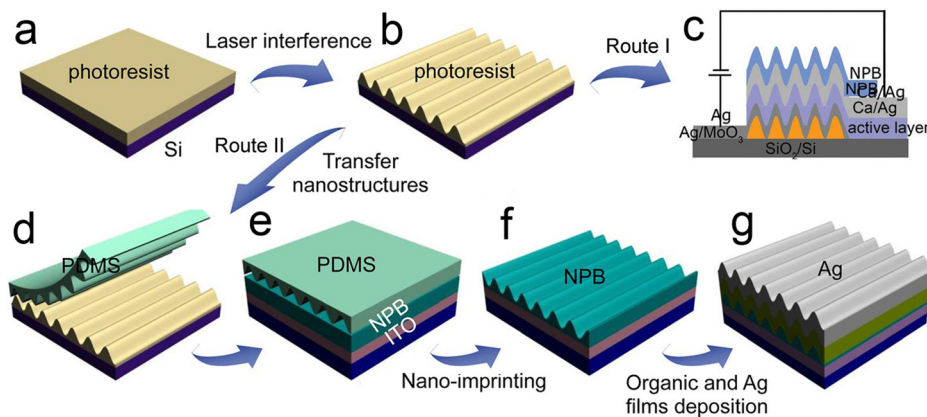


FIG. 11. Route I (a)–(c): (a) spin-coating of the photoresist, (b) introducing periodic nanostructures by interference lithography, and (c) deposition of anode, functional layers, and cathode. Route II (a), (b), and (d)–(g): (d) transfer of the nanostructures to PDMS stamp, (f) imprinting the nanostructures on the hole transparent layer, (f) lifting off PDMS to prepare the nanostructure on the hole transport layer, and (g) depositing the organic and cathode layers. Reproduced with permission from Y. Jin *et al.*, *Adv. Mater.* **24**, 1187–1191 (2012). Copyright 2012 WILEY-VCH Verlag GmbH & Co. KGaA, Weinheim; and from Y. F. Liu *et al.*, *Appl. Phys. Lett.* **109**, 193301 (2016). Copyright 2016 AIP Publishing LLC.

stamp can be duplicated on the hole transport layer of the OLEDs, and the Ag cathode was finally coated to complete the device. According to the emission wavelength, the period of the gratinglike Ag nanostructure is designed to support SPPs resonance at the same wavelength. The luminance and current efficiency are enhanced due to the SPPs-exciton coupling and scattering of the Ag nanostructures. According to the simulation

results, the power loss to the SPP modes can be recovered, thus raising the device efficiency. Additionally, the imprint lithography is also efficient in constructing plasmonic arrays on the phosphor layer of some LEDs device.^{17,23} Generally, the plasmonic arrays supported SLR needs to be precisely designed with respect to the emission wavelength of phosphor to generate desired color and angular enhancement.

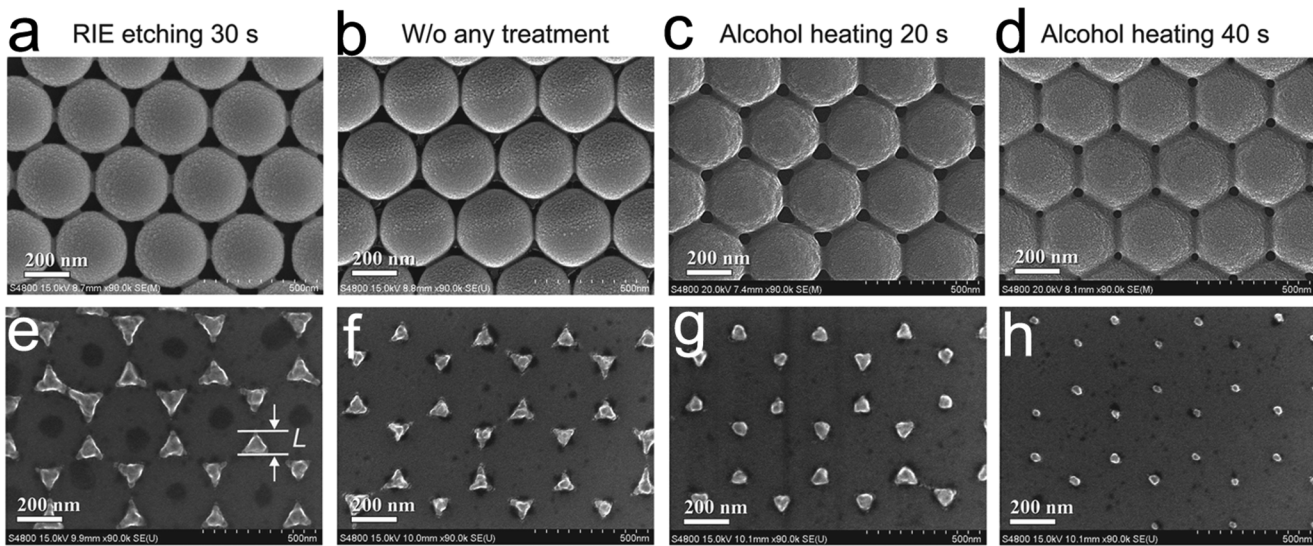


FIG. 12. Fabrication of Al NPs in different sizes by manipulating the gaps of nanosphere templates using one of the following different treatments: (a) reactive ion etching for 30 s, (b) without any treatment, (c) alcohol heating for 20 s, and (d) alcohol heating for 40 s. (e)–(h) The Al NPs fabricated using the nanosphere templates shown in (a)–(d), respectively. Reproduced with permission from J. Yin *et al.*, *Adv. Opt. Mater.* **2**, 451–458 (2014). Copyright 2014 WILEY-VCH Verlag GmbH & Co. KGaA, Weinheim.

E. Template-assisted fabrication

1. Nanosphere lithography

Nanosphere lithography (NSL) technology is often called “colloidal lithography,” which typically uses self-assembled close-packed polymer nanospheres as templates, in combination with reactive ion etching, electrochemical deposition, or vacuum deposition to create textured surfaces or fabricate the desired nanostructures.⁸⁴ NSL is an efficient, economical, and high-throughput fabrication technique for nanostructures while boasting superior structural control and reproducibility. The morphology of templates can be tailored by tuning the size of the nanospheres, annealing-induced deformation, and plasma-etching-driven non-closed packing.^{85–90}

Owing to the flexibility of NSL, periodic plasmonic nanoarrays, including nanodot, nanomesh, and other complex nanostructures, can be directly prepared on the surface of QWs or other layers of LEDs. Yin *et al.*⁹¹ prepared the Al NPs array on AlGaN-based multiple QWs, and by manipulating the morphology

of the nanosphere array, the size of the Al NPs was controlled as shown in Fig. 12. The LSPR peaks of Al NPs array and strong emission enhancement accompanied with large shifts toward shorter wavelengths are observed from the AlGaN QWs with Al NPs. The shift in the emission arising from Al NPs originates from suppression of the ground state exciton emission and enhanced emission from the high-order QWs exciton states by LSP-exciton coupling. When the LSPR frequency matches the higher-order QW excitons, a maximum UV emission enhancement of 3.2-folds is accomplished.

Additionally, NSL has also been employed to pattern the cathode of LEDs to minimize the SPP loss at the dielectric/metal interface. The nanostructured cathode is created by patterning the transparent substrate rather than direct patterning of the cathode. Lee *et al.*⁹² fabricated a plasmonic Ag nanomesh film as the flexible and transparent anode by NSL and vacuum deposition, and the optical transparency of the Ag nanomesh film was optimized by adjusting the diameter of the Ag nanomesh. The nanostructured cathode formed from the periodic nanomesh anode reduces

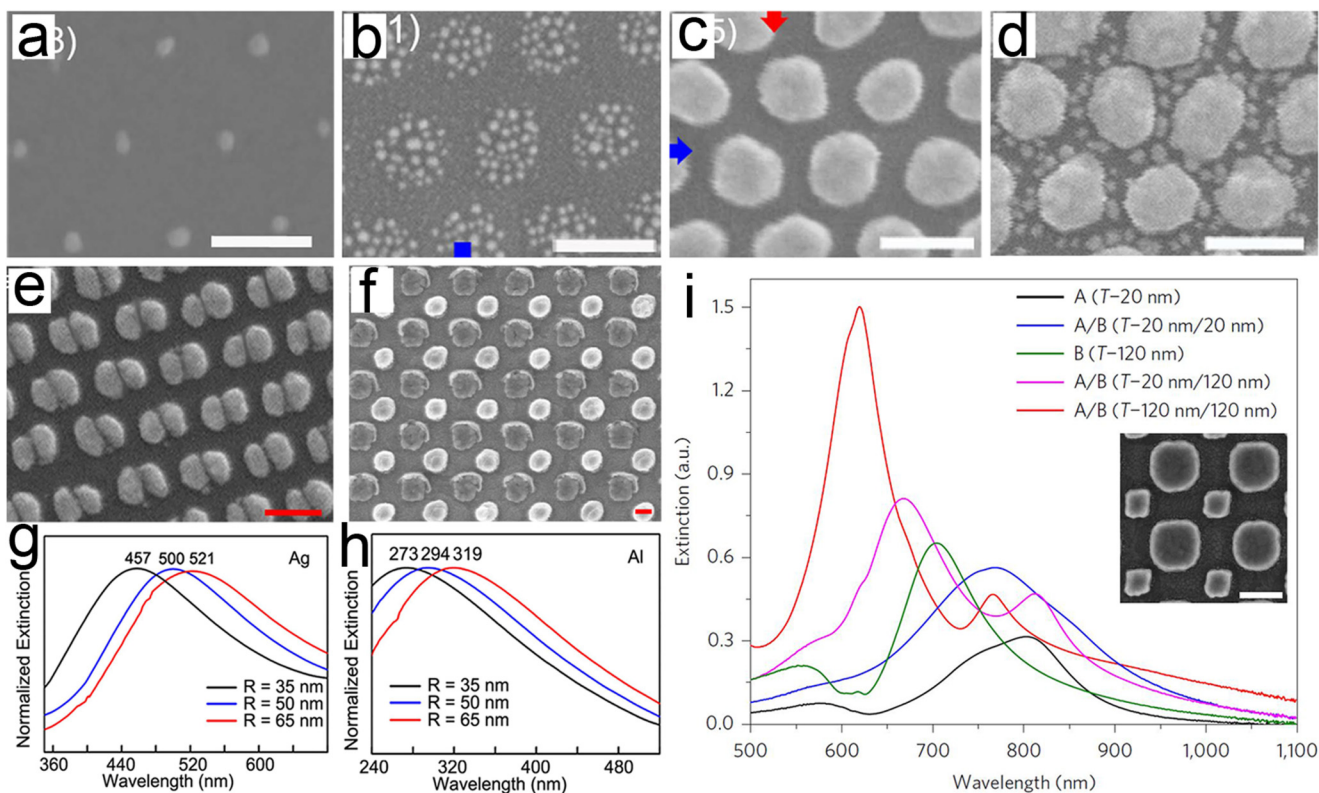


FIG. 13. SEM images of the plasmonic nanoarrays patterned with ultrathin close-packed hexagonal AAO membranes as masks: (a) ultrasmall nanodots, (b) nanoclusters, (c) nanoislands, (d) core-satellites, and (e) nanodimers. (f) SEM image of the binary square and round nanoarrays fabricated with the ultrathin binary pore AAO membrane as the mask (scale bar: 100 nm). Normalized extinction spectra of (g) Ag and (h) Al nanoisland arrays with different nanoisland diameters. (i) Extinction spectra of the binary Ag nanodot arrays on ITO. The inset shows the typical SEM image of the Ag binary nanodot array (scale bar: 200 nm). Reproduced with permission from Q. Hao *et al.*, *Nanotechnology* **28**, 105301 (2017). Copyright 2017 IOP Publishing. Q. Hao *et al.*, *ACS Appl. Mater. Interfaces* **9**, 36199–36205 (2017). Copyright 2017 American Chemistry Society. L. Wen *et al.*, *Nat. Nanotechnol.* **12**, 244–250 (2017). Copyright Nature Publishing Group, 2017.

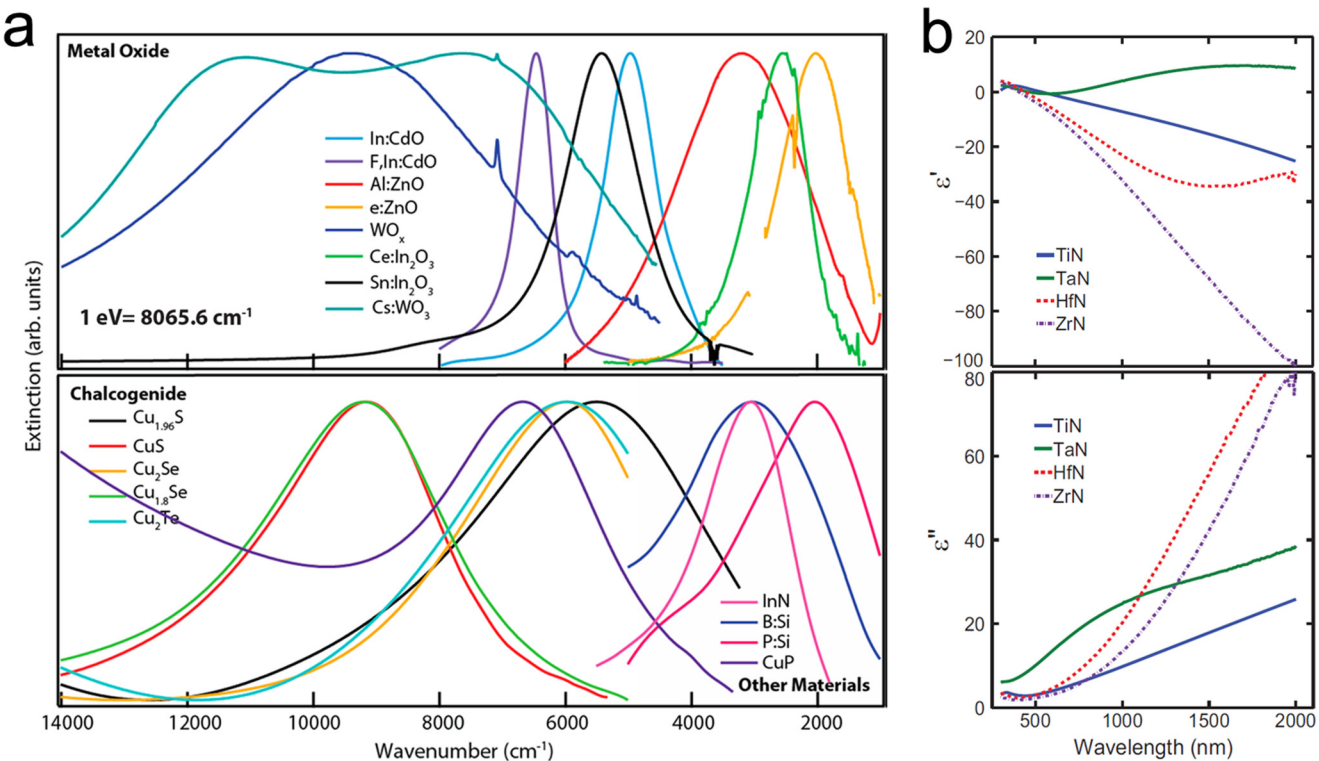


FIG. 14. (a) LSPR in different semiconductor nanocrystals and normalized LSPR extinction spectra of semiconductors spanning the visible and mid-IR regimes. Shown are (top panel) metal oxides such as CdO, ZnO, In₂O₃, and WO_{3-x} and (bottom panel) metal chalcogenides such as Cu_{2-x}E (E = S, Se, Te) as well as Si, metal nitride, and metal phosphide materials, highlighting the variety of semiconducting materials demonstrating LSPR. Reproduced with permission from A. Agrawal *et al.*, Chem. Rev. **118**, 3121–3207 (2018). Copyright 2018 American Chemical Society. (b) The real and imaginary parts of dielectric functions of metal nitride plasmonic materials extracted from spectroscopic ellipsometry measurements. Reprinted with permission from G. V. Naik *et al.*, Opt. Mater. Express **1**, 1090–1099 (2011). Copyright 2011, Optical Society of America.

light loss at the cathode side, resulting in 30% enhancement of the EQE.

2. Anodic aluminum oxide hard-template-assisted lithography

Another commonly used template to produce plasmonic nanoarrays is the anodic aluminum oxide (AAO) membrane, which presents the porous morphology of AAO membranes with the close-packed hexagonal and binary pore structures. The advantages of the AAO membrane are the large patterning area (~cm²), high throughput, and cost-effectiveness. Similar to the NSL, the AAO membranes can be used as deposition masks to produce plasmonic nanoarrays with high spatial resolution, good uniformity, and reproducibility. By changing the mask morphology and deposition conditions, patterned nanoarrays such as nanodot, nanocluster, nanoisland, core-satellites, nanodimers, and binary nanodots array can be created as shown in Figs. 13(a)–13(f).^{93–97} The LSPR from these nanoarrays can be tuned precisely. Figures 13(g) and 13(h) display the extinction spectra of the Ag and Al nanoisland arrays with different sizes produced with ultrathin hexagonal

AAO membranes.⁹³ Figure 13(i) presents the extinction spectra of the Ag binary nanodot arrays prepared with ultrathin binary AAO membranes.⁹⁷ Nevertheless, the full potential of AAO membranes to increase the efficiency of LEDs has not been realized yet. It is possible to pattern plasmonic nanoarrays directly on the carrier injection layers or electrodes of LEDs device by using AAO membrane as the deposition mask.

IV. SUMMARY AND OUTLOOK

LEDs have experienced tremendous development in the past decades due to advantages such as long lifetime, small size, and low energy consumption. They have essentially replaced commercial incandescent light sources and are also gaining ground on fluorescent lightings. New light-emitting materials and novel device configurations are being continuously investigated to obtain highly efficient LEDs for wider commercial implementation. In this Perspective, the challenges and opportunities in QW-based LEDs and OLEDs are described, the plasmonic-based strategies to increase the photon generation and extraction efficiency are discussed, and the plasmonic control over directional emission from

phosphors for directional illumination is introduced. Moreover, important issues pertaining to the design, fabrication, and manipulation of plasmonic structures in LEDs to optimize the light-emitting properties as well as the selection roles in finding appropriate plasmonic materials for desired LEDs devices are explained.

The future trend concerning optimization of plasmonic LEDs is the design of plasmonic structures and the selection of appropriate plasmonic materials. Except plasmonic UV and visible LEDs, the investigation of LEDs device with working wavelength in the near-IR region is receiving growing interest owing to their wide applications in night vision, biomedical imaging, optical communication, and computing. At present, the challenge for near-IR QDs-based LEDs is the PL efficiency and charge transport efficiency of the QDs matrix. Good charge transport is typically accompanied by the generation of highly mobile carriers and exciton dissociation consequently causing self-quenching due to the competition with radiative recombination.⁹⁸ Alternative plasmonic structures beyond noble metal materials may supply a solution to provide good LSPR response in the near-IR region to manage the trade-off between self-quenching and charge transport. The alternative plasmonic materials include degenerately doped metal oxide like Sn:In₂O₃ and In:CdO, metal chalcogenides such as copper-deficient Cu₂S, III-V/Group IV semiconductors such as heavily doped n-type Si, as well as metal nitrides like TiN [as shown in Figs. 1 and 14(a)].^{28–30,99,100–102} In fact, some attempts have been carried out to show their potential in addressing the existed problems in LEDs.^{103,104} Nevertheless, due to the fact that the LSPR response of most conductive semiconducting materials originates from defect-induced carriers, the large carriers scattering by defects generally results in a broadened LSPR and high optical loss into heat, which may seriously limit their applications in the promotion of LEDs performance. For example, TiN and similar plasmonic materials are typically regarded as “metal,” but their high optical loss still holds back the applications in LED devices. Hence, searching for better plasmonic materials with low optical loss is still on the way.

Other than searching for alternative plasmonic materials, another promising approach to optimize and manipulate plasmonic effect is to incorporate dielectric NPs.¹⁰⁵ In fact, the design of dielectric nanostructures on LEDs has been demonstrated effective in promoting LEDs performance owing to their unique low-loss resonant behavior and their ability to scatter in a highly directional manner.^{106–109} These dielectric nanostructures can be potentially employed in fabricating opto-plasmonic optical resonators, where the signal could be further amplified and controlled to improve the LEDs performance.

ACKNOWLEDGMENTS

This work was supported by the National Natural Science Foundation of China (NSFC) (Grant No. 11874108) and City University of Hong Kong Strategic Research Grant (SRG) (Grant No. 7005105). Q. Hao acknowledges the excellent scholar project of Southeast University (Class A).

NOMENCLATURE

AAO = Anodic aluminum oxide

DOS	= Density of states
EBL	= Electron beam lithography
EL	= Electroluminescence
EQE	= External quantum efficiency
IQE	= Internal quantum efficiency
IR	= Infrared
LEDs	= Light-emitting diodes
LEE	= Light extraction efficiency
LSP	= Localized surface plasmon
LSPR	= Localized surface plasmon resonance
NP	= Nanoparticle
NSL	= Nanosphere lithography
OLEDs	= Organic light-emitting diodes
PL	= Photoluminescence
QCSE	= Quantum-confined Stark effect
QD	= Quantum dot
QW	= Quantum well
SLR	= Surface lattice resonance
SPP	= Surface plasmon polariton
SSD	= Solid state dewetting
UV	= Ultraviolet

REFERENCES

1. J. H. Burroughes, D. D. Bradley, A. Brown, R. Marks, K. Mackay, R. H. Friend, P. Burns, and A. Holmes, *Nature* **347**, 539 (1990).
2. S. Nakamura, M. Senoh, and T. Mukai, *Appl. Phys. Lett.* **62**, 2390–2392 (1993).
3. X. Gu, T. Qiu, W. Zhang, and P. K. Chu, *Nanoscale Res. Lett.* **6**, 199 (2011).
4. K. Okamoto, I. Niki, A. Shvartser, Y. Narukawa, T. Mukai, and A. Scherer, *Nat. Mater.* **3**, 601–605 (2004).
5. S. Nakamura and T. Mukai, *Jpn. J. Appl. Phys.* **31**, L1457 (1992).
6. M. A. Baldo, D. O'Brien, Y. You, A. Shoustikov, S. Sibley, M. Thompson, and S. R. Forrest, *Nature* **395**, 151 (1998).
7. Y. Sun, N. C. Giebink, H. Kanno, B. Ma, M. E. Thompson, and S. R. Forrest, *Nature* **440**, 908 (2006).
8. M.-K. Kwon, J.-Y. Kim, B.-H. Kim, I.-K. Park, C.-Y. Cho, C.-C. Byeon, and S.-J. Park, *Adv. Mater.* **20**, 1253–1257 (2008).
9. I.-H. Lee, L.-W. Jang, and A. Y. Polyakov, *Nano Energy* **13**, 140–173 (2015).
10. W. A. Murray and W. L. Barnes, *Adv. Mater.* **19**, 3771–3782 (2007).
11. E. Hutter and J. H. Fendler, *Adv. Mater.* **16**, 1685–1706 (2004).
12. K. Okamoto, I. Niki, A. Scherer, Y. Narukawa, T. Mukai, and Y. Kawakami, *Appl. Phys. Lett.* **87**, 071102 (2005).
13. S. Hayashi and T. Okamoto, *J. Phys. D Appl. Phys.* **45**, 433001 (2012).
14. J. Feng, Y.-F. Liu, Y.-G. Bi, and H.-B. Sun, *Laser Photonics Rev.* **11**, 1600145 (2017).
15. H. Lian, J. Shen, H. Guo, X. Cheng, Q. Dong, J. Yang, and W.-Y. Wong, *Chem. Rec.* **19**, 1753–1767 (2019).
16. G. Lozano, S. R. Rodriguez, M. A. Verschueren, and J. Gómez Rivas, *Light Sci. Appl.* **5**, e16080 (2016).
17. G. Lozano, D. J. Louwers, S. R. K. Rodríguez, S. Murai, O. T. A. Jansen, M. A. Verschueren, and J. Gómez Rivas, *Light Sci. Appl.* **2**, e66 (2013).
18. G. Vecchi, V. Giannini, and J. Gómez Rivas, *Phys. Rev. Lett.* **102**, 146807 (2009).
19. V. Giannini, G. Vecchi, and J. Gómez Rivas, *Phys. Rev. Lett.* **105**, 266801 (2010).
20. V. G. Kravets, A. V. Kabashin, W. L. Barnes, and A. N. Grigorenko, *Chem. Rev.* **118**, 5912–5951 (2018).
21. C. Cherqui, M. R. Bourgeois, D. Wang, and G. C. Schatz, *Acc. Chem. Res.* **52**, 2548–2558 (2019).
22. M. Juodenas, T. Tamulevicius, J. Henzie, D. Erts, and S. Tamulevicius, *ACS Nano* **13**, 9038–9047 (2019).

- ²³G. Lozano, G. Grzela, M. A. Verschuuren, M. Ramezani, and J. Gómez Rivas, *Nanoscale* **6**, 9223–9229 (2014).
- ²⁴M. Ramezani, G. Lozano, M. A. Verschuuren, and J. Gómez Rivas, *Phys. Rev. B* **94**, 125406 (2016).
- ²⁵L. M. Liz Marzán, *Langmuir* **22**, 32–41 (2006).
- ²⁶M. W. Knight, L. Liu, Y. Wang, L. Brown, S. Mukherjee, N. S. King, H. O. Everitt, P. Nordlander, and N. J. Halas, *Nano Lett.* **12**, 6000–6004 (2012).
- ²⁷M. W. Knight, N. S. King, L. Liu, H. O. Everitt, P. Nordlander, and N. J. Halas, *ACS Nano* **8**, 834–840 (2014).
- ²⁸G. V. Naik, V. M. Shalaev, and A. Boltasseva, *Adv. Mater.* **25**, 3264–3294 (2013).
- ²⁹G. V. Naik, J. Kim, and A. Boltasseva, *Opt. Mater. Express* **1**, 1090–1099 (2011).
- ³⁰P. R. West, S. Ishii, G. V. Naik, N. K. Emani, V. M. Shalaev, and A. Boltasseva, *Laser Photonics Rev.* **4**, 795–808 (2010).
- ³¹K. Manthiram and A. P. Alivisatos, *J. Am. Chem. Soc.* **134**, 3995–3998 (2012).
- ³²Y. Yu, Y. Sun, Z. Hu, X. An, D. Zhou, H. Zhou, W. Wang, K. Liu, J. Jiang, and D. Yang, *Adv. Mater.* **31**, 1903829 (2019).
- ³³M. M. Alsaif, K. Latham, M. R. Field, D. D. Yao, N. V. Medehkar, G. A. Beane, R. B. Kaner, S. P. Russo, J. Z. Ou, and K. Kalantar-zadeh, *Adv. Mater.* **26**, 3931–3937 (2014).
- ³⁴J. M. Luther, P. K. Jain, T. Ewers, and A. P. Alivisatos, *Nat. Mater.* **10**, 361–366 (2011).
- ³⁵K. T. Delaney, P. Rinke, and C. G. Van de Walle, *Appl. Phys. Lett.* **94**, 191109 (2009).
- ³⁶E. Kioupakis, P. Rinke, K. T. Delaney, and C. G. Van de Walle, *Appl. Phys. Lett.* **98**, 161107 (2011).
- ³⁷J. Iveland, L. Martinelli, J. Peretti, J. S. Speck, and C. Weisbuch, *Phys. Rev. Lett.* **110**, 177406 (2013).
- ³⁸C.-F. Lu, C.-H. Liao, C.-Y. Chen, C. Hsieh, Y.-W. Kiang, and C. C. Yang, *Appl. Phys. Lett.* **96**, 261104 (2010).
- ³⁹C.-H. Lin, C.-H. Chen, Y.-F. Yao, C.-Y. Su, P.-Y. Shih, H.-S. Chen, C. Hsieh, Y. Kuo, Y.-W. Kiang, and C. C. Yang, *Plasmonics* **10**, 1029–1040 (2015).
- ⁴⁰R. Kour, S. Arya, S. Verma, A. Singh, P. Mahajan, and A. Khosla, *ECS J. Solid State Sci. Technol.* **9**, 015011 (2020).
- ⁴¹S. Nakamura, *Science* **281**, 956–961 (1998).
- ⁴²C.-Y. Chen, Y.-C. Lu, D.-M. Yeh, and C. C. Yang, *Appl. Phys. Lett.* **90**, 183114 (2007).
- ⁴³C.-Y. Cho and S.-J. Park, *Opt. Express* **24**, 7488–7494 (2016).
- ⁴⁴M. Kneissl, T.-Y. Seong, J. Han, and H. Amano, *Nat. Photonics* **13**, 233–244 (2019).
- ⁴⁵D. Li, K. Jiang, X. Sun, and C. Guo, *Adv. Opt. Photonics* **10**, 43 (2018).
- ⁴⁶C.-Y. Cho, Y. Zhang, E. Cicek, B. Rahnema, Y. Bai, R. McClintock, and M. Razeghi, *Appl. Phys. Lett.* **102**, 211110 (2013).
- ⁴⁷J. He, S. Wang, J. Chen, F. Wu, J. Dai, H. Long, Y. Zhang, W. Zhang, Z. C. Feng, J. Zhang, S. Du, L. Ye, and C. Chen, *Nanotechnology* **29**, 195203 (2018).
- ⁴⁸D.-M. Yeh, C.-Y. Chen, Y.-C. Lu, C.-F. Huang, and C. C. Yang, *Nanotechnology* **18**, 265402 (2007).
- ⁴⁹S. Reineke, F. Lindner, G. Schwartz, N. Seidler, K. Walzer, B. Lüssem, and K. Leo, *Nature* **459**, 234 (2009).
- ⁵⁰H. Uoyama, K. Goushi, K. Shizu, H. Nomura, and C. Adachi, *Nature* **492**, 234 (2012).
- ⁵¹Y. Xiao, J. P. Yang, P. P. Cheng, J. J. Zhu, Z. Q. Xu, Y. H. Deng, S. T. Lee, Y. Q. Li, and J. X. Tang, *Appl. Phys. Lett.* **100**, 013308 (2012).
- ⁵²C. Cho, H. Kang, S.-W. Baek, T. Kim, C. Lee, B. J. Kim, and J.-Y. Lee, *ACS Appl. Mater. Interfaces* **8**, 27911–27919 (2016).
- ⁵³M. Yuan, L. N. Quan, R. Comin, G. Walters, R. Sabatini, O. Voznyy, S. Hoogland, Y. Zhao, E. M. Beauregard, P. Kanjanaboons, Z. Lu, D. H. Kim, and E. H. Sargent, *Nat. Nanotechnol.* **11**, 872–877 (2016).
- ⁵⁴J. Song, J. Li, X. Li, L. Xu, Y. Dong, and H. Zeng, *Adv. Mater.* **27**, 7162–7167 (2015).
- ⁵⁵L. Protesescu, S. Yakunin, M. I. Bodnarchuk, F. Krieg, R. Caputo, C. H. Hendon, R. X. Yang, A. Walsh, and M. V. Kovalenko, *Nano Lett.* **15**, 3692–3696 (2015).
- ⁵⁶K. Lin, J. Xing, L. N. Quan, F. P. G. de Arquer, X. Gong, J. Lu, L. Xie, W. Zhao, D. Zhang, C. Yan, W. Li, X. Liu, Y. Lu, J. Kirman, E. H. Sargent, Q. Xiong, and Z. Wei, *Nature* **562**, 245–248 (2018).
- ⁵⁷Y. Cao, N. Wang, H. Tian, J. Guo, Y. Wei, H. Chen, Y. Miao, W. Zou, K. Pan, Y. He, H. Cao, Y. Ke, M. Xu, Y. Wang, M. Yang, K. Du, Z. Fu, D. Kong, D. Dai, Y. Jin, G. Li, H. Li, Q. Peng, J. Wang, and W. Huang, *Nature* **562**, 249–253 (2018).
- ⁵⁸X. Zhang, B. Xu, W. Wang, S. Liu, Y. Zheng, S. Chen, K. Wang, and X. W. Sun, *ACS Appl. Mater. Interfaces* **9**, 4926–4931 (2017).
- ⁵⁹P. Chen, Z. Xiong, X. Wu, M. Shao, Y. Meng, Z. H. Xiong, and C. Gao, *J. Phys. Chem. Lett.* **8**, 3961–3969 (2017).
- ⁶⁰D. K. Gifford and D. G. Hall, *Appl. Phys. Lett.* **81**, 4315–4317 (2002).
- ⁶¹P. A. Hobson, S. Wedge, J. A. Wasey, I. Sage, and W. L. Barnes, *Adv. Mater.* **14**, 1393–1396 (2002).
- ⁶²P. Hobson, J. Wasey, I. Sage, and W. Barnes, *IEEE J. Sel. Top. Quantum Electron.* **8**, 378–386 (2002).
- ⁶³J. Frischeisen, *J. Photonics Energy* **1**, 011004 (2011).
- ⁶⁴Y. Bai, J. Feng, Y.-F. Liu, J.-F. Song, J. Simonen, Y. Jin, Q.-D. Chen, J. Zi, and H.-B. Sun, *Org. Electron.* **12**, 1927–1935 (2011).
- ⁶⁵W. Brüttig, J. Frischeisen, T. D. Schmidt, B. J. Scholz, and C. Mayr, *Phys. Status Solidi A* **210**, 44–65 (2013).
- ⁶⁶Y. Jin, J. Feng, X.-L. Zhang, Y.-G. Bi, Y. Bai, L. Chen, T. Lan, Y.-F. Liu, Q.-D. Chen, and H.-B. Sun, *Adv. Mater.* **24**, 1187–1191 (2012).
- ⁶⁷Y.-G. Bi, J. Feng, Y.-S. Liu, Y.-F. Li, Y. Chen, X.-L. Zhang, X.-C. Han, and H.-B. Sun, *Sci. Rep.* **4**, 7108 (2015).
- ⁶⁸M. C. Gather and S. Reineke, *J. Photonics Energy* **5**, 057607 (2015).
- ⁶⁹Y. F. Liu, M.-H. An, X.-L. Zhang, Y.-G. Bi, D. Yin, Y.-F. Zhang, J. Feng, and H.-B. Sun, *Appl. Phys. Lett.* **109**, 193301 (2016).
- ⁷⁰Z. Liu, S. Liu, K. Wang, and X. Luo, *Appl. Opt.* **49**, 247–257 (2010).
- ⁷¹W. L. Vos, T. W. Tukker, A. P. Mosk, A. Lagendijk, and W. L. IJzerman, *Appl. Opt.* **52**, 2602–2609 (2013).
- ⁷²M. Rycenga, C. M. Cobley, J. Zeng, W. Li, C. H. Moran, Q. Zhang, D. Qin, and Y. Xia, *Chem. Rev.* **111**, 3669–3712 (2011).
- ⁷³Y. Gu, D.-D. Zhang, Q.-D. Ou, Y.-H. Deng, J.-J. Zhu, L. Cheng, Z. Liu, S. T. Lee, Y. Q. Li, and J.-X. Tang, *J. Mater. Chem. C* **1**, 4319 (2013).
- ⁷⁴B. Munkhbat, H. Pöhl, P. Denk, T. A. Klar, M. C. Scharber, and C. Hrelescu, *Adv. Opt. Mater.* **4**, 772–781 (2016).
- ⁷⁵S.-H. Hong, J.-J. Kim, J.-W. Kang, Y.-S. Jung, D.-Y. Kim, S.-Y. Yim, and S.-J. Park, *Nanotechnology* **26**, 385204 (2015).
- ⁷⁶S. H. Kim, T.-S. Bae, W. Heo, T. Joo, K.-D. Song, H.-G. Park, and S. Ryu, *ACS Appl. Mater. Interfaces* **7**, 15031–15041 (2015).
- ⁷⁷C. V. Thompson, *Annu. Rev. Mater. Res.* **42**, 399–434 (2012).
- ⁷⁸D. Kim, A. L. Giermann, and C. V. Thompson, *Appl. Phys. Lett.* **95**, 251903 (2009).
- ⁷⁹X. Fan, Q. Hao, R. Jin, H. Huang, Z. Luo, X. Yang, Y. Chen, X. Han, M. Sun, Q. Jing, Z. Dong, and T. Qiu, *Sci. Rep.* **7**, 2322 (2017).
- ⁸⁰S. Yang, F. Xu, S. Ostendorp, G. Wilde, H. Zhao, and Y. Lei, *Adv. Funct. Mater.* **21**, 2446–2455 (2011).
- ⁸¹S.-H. Chuang, C.-S. Tsung, C.-H. Chen, S.-L. Ou, R.-H. Horng, C.-Y. Lin, and D.-S. Wuu, *ACS Appl. Mater. Interfaces* **7**, 2546–2553 (2015).
- ⁸²A. Le Bris, F. Maloum, J. Teisseire, and F. Sorin, *Appl. Phys. Lett.* **105**, 203102 (2014).
- ⁸³C.-H. Lu, C.-C. Lan, Y.-L. Lai, Y.-L. Li, and C.-P. Liu, *Adv. Funct. Mater.* **21**, 4719–4723 (2011).
- ⁸⁴J. C. Hulteen and R. P. Van Duyne, *J. Vac. Sci. Technol. A* **13**, 1553–1558 (1995).
- ⁸⁵L. Li, T. Zhai, H. Zeng, X. Fang, Y. Bando, and D. Golberg, *J. Mater. Chem.* **21**, 40–56 (2011).
- ⁸⁶Z. Yi, G. Niu, J. Luo, X. Kang, W. Yao, W. Zhang, Y. Yi, Y. Yi, X. Ye, T. Duan, and Y. Tang, *Sci. Rep.* **6**, 32314 (2016).

- ⁸⁷A. Kosiorek, W. Kandulski, H. Glaczynska, and M. Giersig, *Small* **1**, 439–444 (2005).
- ⁸⁸A. Valsesia, T. Meziani, F. Bretagnol, P. Colpo, G. Ceccone, and F. Rossi, *J. Phys. D Appl. Phys.* **40**, 2341–2347 (2007).
- ⁸⁹Z. Dai, X. Xiao, L. Liao, J. Zheng, F. Mei, W. Wu, J. Ying, F. Ren, and C. Jiang, *Appl. Phys. Lett.* **103**, 041903 (2013).
- ⁹⁰J. Zheng, Z. Dai, F. Mei, X. Xiao, L. Liao, W. Wu, X. Zhao, J. Ying, F. Ren, and C. Jiang, *J. Phys. Chem. C* **118**, 20521–20528 (2014).
- ⁹¹J. Yin, Y. Li, S. Chen, J. Li, J. Kang, W. Li, P. Jin, Y. Chen, Z. Wu, J. Dai, Y. Fang, and C. Chen, *Adv. Opt. Mater.* **2**, 451–458 (2014).
- ⁹²S.-M. Lee, Y. Cho, D.-Y. Kim, J.-S. Chae, and K. C. Choi, *Adv. Opt. Mater.* **3**, 1240–1247 (2015).
- ⁹³Q. Hao, H. Huang, X. Fan, X. Hou, Y. Yin, W. Li, L. Si, H. Nan, H. Wang, Y. Mei, T. Qiu, and P. K. Chu, *Nanotechnology* **28**, 105301 (2017).
- ⁹⁴Q. Hao, H. Huang, X. Fan, Y. Yin, J. Wang, W. Li, T. Qiu, L. Ma, P. K. Chu, and O. G. Schmidt, *ACS Appl. Mater. Interfaces* **9**, 36199–36205 (2017).
- ⁹⁵Q. Hao, J. Pang, Y. Zhang, J. Wang, L. Ma, and O. G. Schmidt, *Adv. Opt. Mater.* **6**, 1700984 (2018).
- ⁹⁶Q. Hao, W. Li, H. Xu, J. Wang, Y. Yin, H. Wang, L. Ma, F. Ma, X. Jiang, O. G. Schmidt, and P. K. Chu, *Adv. Mater.* **30**, 1705421 (2018).
- ⁹⁷L. Wen, R. Xu, Y. Mi, and Y. Lei, *Nat. Nanotechnol.* **12**, 244–250 (2017).
- ⁹⁸H. Lu, G. M. Carroll, N. R. Neale, and M. C. Beard, *ACS Nano* **13**, 939–953 (2019).
- ⁹⁹A. Agrawal, S. H. Cho, O. Zandi, S. Ghosh, R. W. Johns, and D. J. Milliron, *Chem. Rev.* **118**, 3121–3207 (2018).
- ¹⁰⁰C. Coughlan, M. Ibanez, O. Dobrozhana, A. Singh, A. Cabot, and K. M. Ryan, *Chem. Rev.* **117**, 5865–6109 (2017).
- ¹⁰¹X. Liu and M. T. Swihart, *Chem. Soc. Rev.* **43**, 3908–3920 (2014).
- ¹⁰²X. Fan, M. Li, Q. Hao, M. Zhu, X. Hou, H. Huang, L. Ma, O. G. Schmidt, and T. Qiu, *Adv. Mater. Interfaces* **6**, 1901133 (2019).
- ¹⁰³I. E. Fragkos and N. Tansu, *Sci. Rep.* **8**, 13365 (2018).
- ¹⁰⁴Y.-J. Lu, R. Sokhoyan, W.-H. Cheng, G. Kafae Shirmanesh, A. R. Davoyan, R. A. Pala, K. Thyagarajan, and H. A. Atwater, *Nat. Commun.* **8**, 1631 (2017).
- ¹⁰⁵A. I. Kuznetsov, A. E. Miroshnichenko, M. L. Brongersma, Y. S. Kivshar, and B. Luk'yanchuk, *Science* **354**, aag2472 (2016).
- ¹⁰⁶X. Zhu, Y. Ou, V. Jokubavicius, M. Syväjärvi, O. Hansen, H. Ou, N. A. Mortensen, and S. Xiao, *Appl. Phys. Lett.* **101**, 241108 (2012).
- ¹⁰⁷G. Kang, J. Yoo, J. Ahn, and K. Kim, *Nano Today* **10**, 22–47 (2015).
- ¹⁰⁸S. Gorsky, R. Zhang, A. Gok, R. Wang, K. Kebede, A. Lenef, M. Raukas, and L. Dal Negro, *APL Photonics* **3**, 126103 (2018).
- ¹⁰⁹B. H. Bae, S. Jun, M. S. Kwon, Y. W. Park, C. J. Han, S.-I. Kim, and B.-K. Ju, *Opt. Mater.* **92**, 87–94 (2019).